



Using a discrete element approach to model lava dome emplacement and collapse

Claire E. Harnett^{a,*}, Mark E. Thomas^a, Matthew D. Purvance^b, Jurgen Neuberg^a

^a Institute of Geophysics and Tectonics, University of Leeds, Leeds LS2 9JT, UK

^b Itasca Consulting Group, Minneapolis, MN 55401, USA



ARTICLE INFO

Article history:

Received 7 March 2018

Received in revised form 12 June 2018

Accepted 20 June 2018

Available online 25 June 2018

Keywords:

Lava dome

Emplacement dynamics

Collapse

Discrete element modelling

ABSTRACT

Lava dome collapses can lead to explosive activity and pyroclastic flow generation which makes them one of the most deadly consequences of volcanic activity. The mechanisms linked to a collapse are however still poorly understood and very few numerical models exist that investigate the actual collapse of a lava dome after emplacement. We use a discrete element method implemented in the modelling software *Particle Flow Code* to investigate lava dome growth, but also go further to test the stability of the dome under the following conditions: increased internal pressure; switch in extrusion direction caused by partial cooling of the dome; and extrusion of lava onto variable underlying topography. We initially show the morphology development of a growing lava dome, and how the rheological boundary between core and talus evolves throughout the lifetime of a dome and with varied solidus pressures. Through visualisation of strain accumulation within the lava dome we show superficial rockfall development due to interaction with topography, whereas large deep-seated failures occur when the dome is exposed to internal overpressures. We find that a switch in extrusion direction promotes a transition from endogenous to exogenous dome growth and leads to lava lobe formation. We demonstrate that lava dome collapse exhibits many features similar to common landslides and by investigating strain patterns within the dome, we can use numerical modelling to understand features that elude field observations.

© 2018 The Authors. Published by Elsevier B.V. This is an open access article under the CC BY license (<http://creativecommons.org/licenses/by/4.0/>).

1. Introduction

Lava domes form when magma extrudes from a vent and piles up due to its high viscosity. Once unstable, collapse of a lava dome can generate rockfalls, debris avalanches, and pyroclastic flows. Despite this significant hazard, relationships between active dome extrusion and collapse processes are still not entirely understood (Calder et al., 2002; Voight, 2000).

The stability of a lava dome is affected by multiple factors including but not limited to: gravitational collapse due to over-steepening (Swanson et al., 1987); internal gas overpressures (Elsworth and Voight, 2001; Sparks, 1997; Voight and Elsworth, 2000); interaction with intense rainfall (Carn et al., 2004; Elsworth et al., 2004; Matthews et al., 2002; Taron et al., 2007); a switch in extrusion direction (Loughlin et al., 2010); topography underlying the dome (for example, a dome exceeding the size of the crater in which it sits) (Voight et al., 2002); hydrothermal alteration (Ball et al., 2015); and the fracture state of the dome, both small-scale due to dynamic and explosive dome growth (e.g. Darmawan et al., 2018) and large scale from local tectonic faulting (e.g. Walter et al., 2015).

Dome morphology also plays an inevitable role in overall dome stability. Different types of domes have been classified by various studies (e.g. Blake, 1990; Watts et al., 2002), ranging from “pancake” domes, coulées, and lava lobes (generally wide and low in height) to Peleean or blocky domes, which have a more extensive talus apron and are taller for a given radius (Blake, 1990). Blocky domes can also generate spines, whereby stiff, cooled material extrudes near-vertically (Watts et al., 2002). Blockier/Peleean-style domes are more likely to collapse due to the larger height to radius ratio, and collapses generally involve more material than shallow collapses at pancake-style domes (Blake, 1990). The domes modelled in this paper are analogous to blockier domes, rather than “pancake” domes or coulées.

Despite recent advances in computational modelling of lava domes (Hale, 2008; Hale et al., 2007, 2009a; Husain et al., 2014, 2018), current models focus on understanding initial emplacement dynamics rather than more hazardous aspects of dome collapse. Here we develop the idea, first posed by Husain et al. (2014), of using discrete element method (DEM) modelling to reproduce both the emplacement and instability of a lava dome with intermediate silica composition. Previous dome emplacement simulations have mostly employed the finite element method (FEM) (Bourgouin et al., 2007; Hale, 2008; Hale et al., 2009a, 2009b; Hale and Wadge, 2008), whereby it is computationally expensive to introduce additional perturbing factors with the intention

* Corresponding author.

E-mail address: eeceh@leeds.ac.uk (C.E. Harnett).

of initiating collapse. By using a DEM model, we are able to start with an initial dome emplacement and apply, in several model scenarios, different mechanisms attributed to dome collapse in the literature. We intend this to be a pilot study to illustrate the potential of the model in simulating dome growth, morphology and collapse, and show this model can be applied in more specific locations with exact scenarios or conditions.

2. Methodology

2.1. Discrete element method

We use Particle Flow Code (PFC), a commercial software developed by Itasca (2017), to undertake a two-dimensional analysis of dome growth and collapse. PFC uses the discrete element method (Cundall and Strack, 1979) to simulate an assembly of individual particles that behave as rigid bodies carrying a force and moment that are updated per model time step. The particles interact via contact bonds, defined by individual contact models, which act as point (“parallel” bonds) or beam (“flatjoint” bonds) style connections between particles (Fig. 1). Bond behaviour is primarily governed by the normal stiffness (k_n – incompressibility) and shear stiffness (k_s) associated with the contact interface, although the bonds also have attributed values for cohesion, tensile strength, and friction. Bond breakage occurs if the tensile or shear strength of the contact is exceeded, which is used to represent damage in the model material. PFC calculates an explicit solution to Newton’s laws of motion, thus limiting the need to dictate additional particle behaviours (Potyondy, 2016). Each particle in this case is not intended to represent an individual crystal or a block of rock, but rather a discrete element for the purpose of computation.

DEM is commonly used to study soil and rock mechanics (Wang and Tonon, 2009; Zhang et al., 2011), civil engineering scenarios (Jenck et al., 2009; Wang et al., 2003), and more recently the field of volcanology, to study volcanic processes such as gravitational spreading (Morgan and McGovern, 2005a, 2005b), caldera collapse (Gudmundsson et al., 2016; Holohan et al., 2011, 2015), and lava dome growth (Husain et al., 2014, 2018). This study differs to previous DEM models of lava dome emplacement (Husain et al., 2014), in that we incorporate new bonding methods in PFC to better represent dome rock properties and explicitly test conditions associated with dome collapse.

2.2. Model description

We model a simplified internal dome structure comprising two main units: (1) a frictionless, ductile core and (2) an outer friction-controlled talus region. We use the term talus to refer to any dome material that is behaving as rock and do not distinguish between talus slopes that have become detached from the dome and the intact crust of the dome. It is likely there is a transition zone between the core and talus regions, often termed the carapace (e.g. Wadge et al., 2009), however for simplicity this is not included here as a separate region. This assumption is based on studies suggesting an abrupt rheological change when melt develops a critical crystal content, thus exhibiting material strength that can be characterised as a solid (Cordonnier et al., 2012).

A thermal imaging study by Hutchison et al. (2013) showed the outer crust of the dome appears to behave dynamically during dome growth, rather than acting as a stiff, rigid layer. DEM allows the talus to deform independently without imposing a rigid boundary upon the model region, suggesting this method is appropriate for modelling the evolution of both the fluid and solid portions of lava domes.

We do not implement an explicit mechanism for magma reaching the surface, and instead the dome grows through a constant supply of magma into the interior. After initial extrusion conditions are applied the dome is free to grow “naturally” and this can lead to exogenous spine generation. As with previous dome emplacement simulations (e.g. Hale, 2008), we note that our model is best applied to the analysis of large, whole-dome processes, hence localised flow processes are not fully considered.

The model is initialised by generating a “batch” of magma in the conduit which is followed by a constant supply of fresh magma. At model initialization, particles are packed within the conduit to ensure that contacts exist at all particle-particle interfaces. Packing is random to avoid hexagonal particle packing (Potyondy, 2016), as this can lead to unreliable model behaviour. This packing introduces a randomness to the dome geometry in each model run and leads to dome asymmetry. After magma exits the conduit, its behaviour is governed by: (a) the driving force due to velocity of conduit material; (b) the downward force of gravity; and (c) the force and moment transfer from particle-particle interactions. The magma is driven by an upwards velocity of 2 m/s; this is kept constant in all models as we do not focus on the effect of extrusion rate on dome growth. Mapping this 2D ascent velocity to a 3D extrusion rate would give faster extrusion rates than those used in other discrete element models (Hungri et al., 2014; Husain et al., 2018), however to reduce computation time we simulate a fast end member of extrusion. We note that our simulations run close to real time and therefore a modelled dome would take months to extrude at low ascent velocities, thus we accelerate the extrusion process and do not explicitly compare modelled timescales to real world observations.

Identifying the transition of ductile core material to talus is crucial in a lava dome emplacement model, as relative core/talus volumes influence dome morphology and therefore stability (Hale et al., 2009a). The solidification of magma is primarily controlled by two mechanisms: the cooling of the lava surface which leads to a solid crust and rheological stiffening, and volatile exsolution caused by decompression which increases liquidus temperature and therefore promotes crystallisation. Lava domes most commonly form in andesitic-dacitic lavas (Ogburn et al., 2015), where solidification of lava is dominated by degassing-induced crystallisation (Sparks et al., 2000). Cooling can therefore be considered negligible in the solidification process; we follow the example of previous dome emplacement models (Hale, 2008; Husain et al., 2014; Simmons et al., 2005) and employ the solidus pressure to mark the transition of magma from a liquid to a crystallised solid state:

$$T_{\text{liq,sol}} = a_T + b_T \ln(p) + c_T \ln(p)^2 + d_T \ln(p)^3, \quad (1)$$

where T gives the liquidus and solidus temperatures (Fig. 2), a_T , b_T , c_T and d_T are constants (Couch et al., 2003; Melnik and Sparks, 2005),

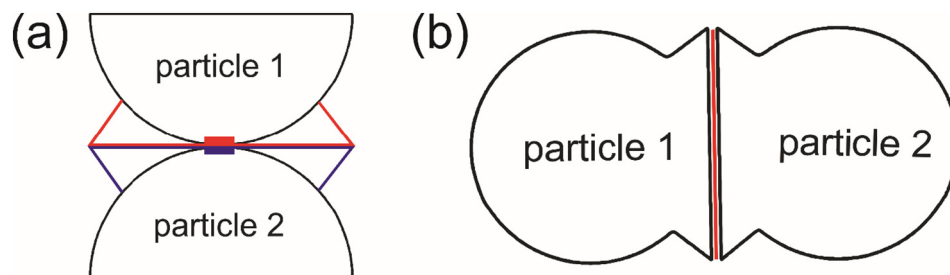


Fig. 1. (a) A parallel bond in PFC; (b) a flatjoint bond in PFC, showing skirted particle geometry.

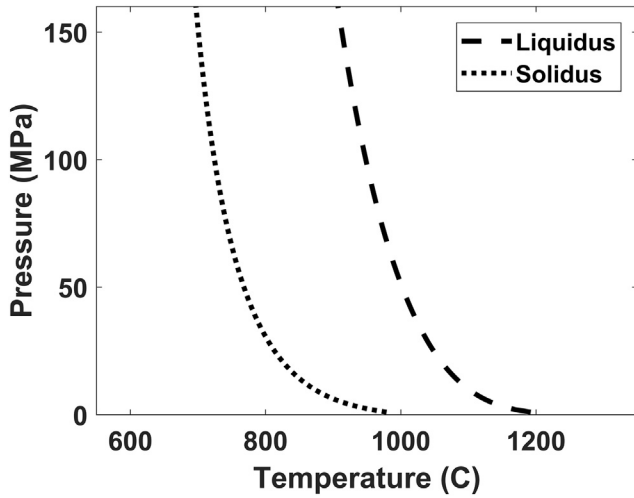


Fig. 2. Temperature-pressure curve showing magma solidus using Eq. (1) derived by Couch et al. (2003) for initial SHV melt composition.

and p is pressure. Melnik and Sparks (2005) use the initial melt composition at Soufrière Hills volcano (SHV) (Couch et al., 2003) to experimentally establish the solidus and liquidus temperatures; the best fit to this experimental data derives the constants a_T , b_T , c_T and d_T .

Studies on lava from SHV, a volcano with numerous cycles of dome growth and collapse (Wadge et al., 2010), suggest variable properties (e.g. Matthews and Barclay, 2004; Voight et al., 2006) with temperatures ranging from 830 °C to 940 °C. The method from Moore et al. (1998) establishes that water content is negligible for the given temperature range and composition. In our model we assume melt experiences perfect volatile loss at the conduit exit and is dry at the time of emplacement, consistent with low (<0.12%) water contents measured in groundmass from the 1995–1996 Soufrière Hills dome (Villemant et al., 2008). The solidus pressure is therefore between 0.1 MPa and 5 MPa, dependent on temperature (Hale, 2008). In a dynamically evolving dome system, it is likely that the solidus pressure evolves too. For model simplicity, we use a fixed value (0.4 MPa) in the starting condition for all collapse models, but we also include a sensitivity analysis of the solidus pressure on core/talus proportions within the dome (Section 3.1).

The so-called “level set method” (Osher and Sethian, 1988) is a numerical method previously incorporated into FEM simulations to track the interface between interior core and outer talus regions (Hale et al., 2007; Hale and Wadge, 2005, 2008). The evolution of this interface, where important rheological changes occur, is critical to dome stability. Hale et al. (2007) presented the benefits of using the level set method in FEM models of lava domes, as it allows both the core/talus interface and the flow front to be tracked without remeshing and therefore reduces computational expense. However when Husain et al. (2014) applied this method to DEM models, it resulted in an unlikely morphology of the core/talus boundary. Therefore, instead of using the level set method we simply calculate the maximum principal stress (σ_1) (Jaeger et al., 2009) on each discrete particle and adapt the particle properties according to when each particle reaches the solidus pressure.

$$\sigma_1 = \frac{1}{2}(\sigma_{xx} + \sigma_{yy}) + \left[\sigma_{xy}^2 + \frac{1}{4}(\sigma_{xx} - \sigma_{yy})^2 \right]^{\frac{1}{2}} \quad (2)$$

It is important to note that this transition in properties is unidirectional, so although solidification is considered in the model, re-melting cannot occur. Determining the equivalent particle properties of the ductile core material is challenging as a calibration procedure cannot be performed. We therefore use the micro-properties obtained by Husain et al. (2014) through sensitivity analyses. The study focused

particularly on determining the effect of cohesion and bond stiffness on material behaviour. We correlate the parallel bond stiffness of the core material to magma viscosity by

$$\eta = k_s \Delta t y, \quad (3)$$

where η is viscosity, k_s is the shear stiffness of the bond, t is the model time step, and y is the unit length of the material (i.e. particle size). Variation in magma viscosity at SHV can span up to eight orders of magnitude (Couch et al., 2003; Melnik and Sparks, 2002; Voight et al., 1999); to simplify our model we assume a constant viscosity of 10^8 Pa in all models and do not vary the micro-properties of the magma material (for a complete list of model parameters, see Supplementary Material A).

For the ductile portion of the model we use a parallel bonded contact model, as the point-style contact does not inhibit rotational resistance and therefore provides the behaviour of a fluid. When an individual particle reaches the solidus pressure, the bond type is updated to a flatjoint bond (Potyondy, 2012), where a beam-style contact changes the geometry of the interface so that the particles become “skirted” in shape (Fig. 1). Recent numerical studies have shown that by incorporating this type of particle bond, the material acts more like a solid rock than the more conventional contact models in earlier versions of PFC. This is due to the increased interlocking and maintenance of rotational resistance, even after a contact is broken (Wu and Xu, 2016). Using the flat jointed contact model overcomes many problems seen in earlier PFC studies (Cho et al., 2007; Holohan et al., 2011), and ensures the material is acting like a solid rock in both compression and tension.

We can use analogue models to evaluate the strain field and likely flow structures within a dome, thereby verifying the modelled geometries. Buisson and Merle (2002) show that flow in the central region of the dome above the conduit is dominated by material ascent due to the driving force of injected magma. Flow in the lateral portions of the dome is primarily horizontal or downward and governed only by gravity. By tracing particle velocities in PFC, we show that our model replicates this well (Fig. 3). We also compare this flow structure to dome growth identified by Walter et al. (2013) using pixel offsets, where growth directly above the conduit is dominated by upward and vertical movement of magma, and flow in the lateral portions of the dome is primarily away from the conduit and gravity-controlled.

2.3. Strain modelling

Due to the heterogeneity of displacements in a particle-based model, it can be challenging to establish a link between individual particle displacements and macro-level strain. To bridge this gap, we perform inverse strain modelling (i.e. fitting a strain model to displacement data) in order to visualise localised strain (Morgan and McGovern, 2005a, 2005b; Holohan et al., 2011). This method (Schöpfer et al., 2006) assumes a continuum and the nearest neighbours of each particle are

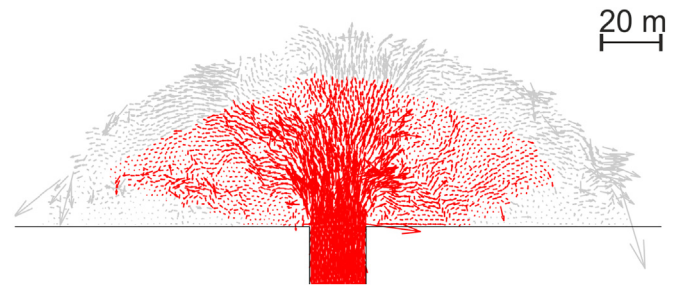


Fig. 3. Velocity vectors during dome growth, where red is core material and grey is talus material. The relative velocity magnitude is proportional to arrow size, where conduit material has a velocity of 2 m.

identified and their positions tracked across a given time step. The average displacements are used to calculate a displacement gradient tensor, which can be used to determine the Cauchy-Green deformation tensor. We use the deformation gradient tensor to compute maximum shear strain using

$$\gamma_{\max} = \frac{\lambda_{\max} - \lambda_{\min}}{2(\lambda_{\max} * \lambda_{\min})^{\frac{1}{2}}}, \quad (4)$$

where γ_{\max} is the maximum shear strength, and λ represents the maximum and minimum eigenvalues of the deformation gradient tensor (Cardozo and Allmendinger, 2009). We note that we do not consider particle rotation, instead calculating strain based on absolute displacement of each particle centroid. In many cases particles in the models have particularly large strains, for example when a particle “rolls” down the side of the edifice, simulating a small scale rock fall. These large strains hide smaller strains occurring within the dome, so we plot a strain cut-off criterion in each of our model figures. Shear strains are then normalised to emphasise the relative shear strain in each model. This allows distinction of where material moves along a boundary (e.g. a fault or a shear plane) from material moving as a block and is particularly relevant in the case of collapse models as calculating finite strain can allow identification of developing failure planes.

3. Model results

In this section, we first focus on the emplacement of a lava dome, followed by sensitivity analyses of dome morphology to both solidus pressure and conduit width. We create a dome emplacement model and use this as a starting condition, enabling application of external factors observed to trigger pyroclastic flow generation or dome collapse. In this initial study, we do not model rainfall-induced collapse due to varied hypotheses for how addition of rainfall to the volcanic system leads to collapse (Matthews and Barclay, 2004). We therefore focus on simulating the following triggering mechanisms: pressurisation of the dome, a switch in extrusion direction, and topography-controlled collapses.

3.1. Dome emplacement

Running a simple dome emplacement model shows a morphology with steep sides and a flatter area towards the apex of the dome (Fig. 4). At the beginning of dome growth (Fig. 4a), only solid material is extruded as there is no overburden pressure to maintain fluid core material within the dome. Over time, a fluid core is encapsulated by a solid outer talus region (Fig. 4b). At the base of the dome there are regions where core material overrides solid talus material (Fig. 4c). Although not investigated further here, presence of a talus substrate beneath the core may have significant impacts on overall dome stability. An area of the dome where core material spreads over underlying talus material can be unstable and cause more explosive activity during retrogressive collapse (Hale et al., 2009a; Herd et al., 2005).

The solidus pressure influences talus thickness, as higher pressures result in a smaller core volume fraction. While our primary models use a solidus pressure of 0.4 MPa, we also show emplaced domes with solidus pressures of 0.2 MPa and 0.8 MPa to demonstrate the effect of solidus pressure on dome morphology (Fig. 5), and the potential effects of this are discussed further in Section 4.4. We observe that higher relative talus volume (Table 1) also results in steeper dome morphology (Fig. 5).

3.2. Sensitivity of dome morphology to conduit diameter

Lava domes vary in morphology due to rheological and mechanical properties (e.g. Blake, 1990; Calder et al., 2015; Watts et al., 2002). Blake (1990) documented variations in observed dome heights from 8 m to 243 m, and radius variations of 20 m to 1093 m. The models in this paper are extruded from a conduit with diameter of 20 m, and reach a height of 70 m and width of 210 m, where the dome height limit appears to have been reached, and any magma addition results only in lateral spreading (Supplementary Material B: animation of dome emplacement). Considering the same rheology, solidus pressure of 0.4 MPa, extrusion rate, and material properties (Fig. 6), we use a larger conduit of 50 m to test whether the dome geometry is independent of magma input. The 50 m conduit results in a dome that is 110 m tall, and 340 m wide; this is again approximately a 1:3 height-to-width ratio. Hence we determine that lava dome morphology is insensitive to conduit diameter, and therefore the models with a conduit diameter of 20 m are indicative of process and morphology at varying scales.

There are similar dome morphologies found between the models with varying conduit diameters. There is also a similar geometry to the core/talus interface, particularly at the base of the dome where both models show core material underlain by talus material. The main difference between the results is the proportion of core to talus. In the model with a 20 m conduit, we see 43% talus and 57% core, whereas in the model with a 50 m conduit, we see 23% talus and 77% core material. This can be explained by a low solidus pressure (0.4 MPa) resulting in only a thin shell required to encase the ductile material in the interior of the dome.

Core volume fraction was also estimated by Hale et al. (2009a, 2009b) using FEM simulations, with values of core volume ranging from 26% to 66%. Estimates were made from ground-based radar measurements at SHV (Wadge et al., 2008) and showed that a surprisingly low proportion (39%) of the extruded lava remained in the core. We suggest that our relative overestimates of core proportion arise from simulating one continuous extrusion period, rather than a more realistic periodic extrusion. The pauses during periodic extrusion allow further solidification to occur, increasing talus volume. Estimates of talus thickness are difficult to obtain during active dome extrusion. Dzurisin et al. (1990) used magnetization to estimate outer layer thickness of the Mount St. Helens dome as 10–30 m thick. In the 20 m conduit model, we find a talus thickness of 13–23 m (considering only where talus overlies core, and not the distal talus aprons), and for the 50 m conduit model, talus thicknesses range from 15 to 20 m. This suggests we have

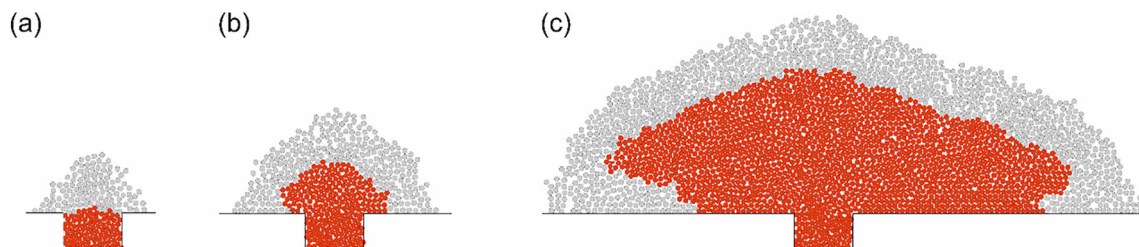


Fig. 4. Snapshots of growth at (a) 5% of final growth, (b) 15% of final growth and (c) 100% of final growth; red particles shows liquid, parallel-bonded core and grey particles shows solid, flat-jointed talus. Solidus pressure = 0.4 MPa. For further information on dynamic growth, see video in Supplementary Material B.

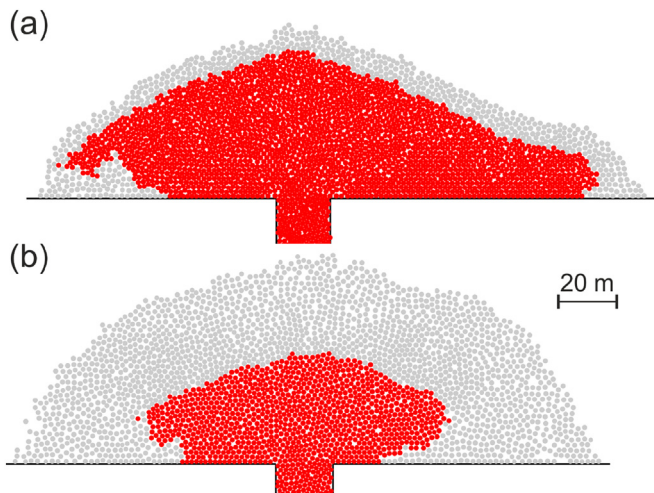


Fig. 5. PFC dome model emplaced with solidus pressures of (a) 0.2 MPa and (b) 0.8 MPa. Growth state corresponds to 100% of growth in Fig. 4. Red particles show liquid, parallel-bonded core and grey particles show solid, flat-jointed talus.

good estimates of talus encasing the core, but could be underestimating talus apron volume.

Despite differences in relative core/talus volumes, the overall shape of the rheological boundary is very similar to that suggested in conceptual models (Hutchison et al., 2013) and existing FEM models (Hale et al., 2009a, 2009b). This confirms our lava dome emplacement model is valid, providing a good starting condition from which to test collapse mechanisms.

3.3. Gravity and renewed pressurisation of the dome

Dome collapses are frequently followed by explosive eruptions, suggesting that internal pressurisation is likely to play a role in triggering instabilities in lava domes. This was observed particularly at SHV following collapses in September 1996 and June, August and September 1997 (Cole et al., 1998; Voight and Elsworth, 2000). Pyroclastic flow generation has also been observed in conjunction with gas pressurisation at Mt. Unzen (Sato et al., 1992). Tilt deformation prior to dome collapse events also suggests shallow pressurisation and links timing of collapse to maximum pressurisation (Elsworth and Voight, 2001).

Voight and Elsworth (2000) modelled a hemispherical dome above a pressurised conduit and calculated gas pressure diffusion across the dome. They define an isolated block using an inclined arbitrary basal sliding plane, upon which the uplift pressures act. This allows calculation of the factor of safety (a measure of stability defined as the ratio of resisting to disturbing forces) for the isolated and potentially unstable block. The model shows a dome can remain stable in the early stages of pressurisation and not fail until subsequent pulses of pressure are applied to the dome. The authors explain this by suggesting the pressure on the critical failure surface must exceed a given threshold, and this may require several oscillations. Previous studies (Robertson et al.,

Table 1

Relative core/volume fraction, expressed as a percentage of total extruded material, for solidus pressures of 0.2 MPa, 0.4 MPa and 0.8 MPa. Model parameters for these simulations are listed in Supplementary Material A.

Solidus	100% of growth	
	Core (%)	Talus (%)
0.2 MPa	79.0	21.0
0.4 MPa	37.3	62.7
0.8 MPa	34.8	65.2

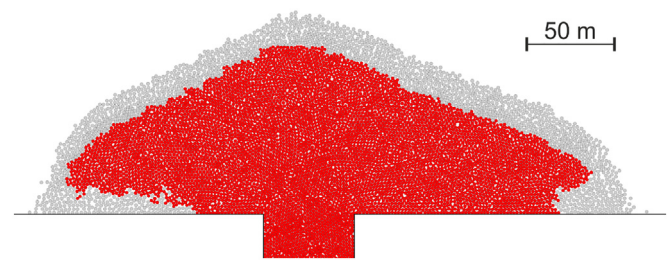


Fig. 6. PFC dome model emplaced with a 50 m conduit, and solidus pressure of 0.4 MPa, where red represents core material and grey represents talus material.

1998; Voight et al., 1998) find gas pressurisation magnitudes of ~10 MPa, and Voight and Elsworth (2000) find decompression of a dome core by 2–5 MPa can lead to explosive activity.

We aim to exploit the advantages of a DEM model by establishing whether it is possible to create a failure surface, rather than examining the effect of pressure on a geometrically simplified pre-existing weakness. After stopping extrusion, we apply an upward force within a hemispherical region above the conduit (where the diameter of this region is equivalent to conduit width), to act as a renewed pressurisation of the system. We add the force in this region due to observations which suggest that processes controlling the dome pressurisation are shallow-level, either deep within the dome interior or in the shallow conduit (Sparks, 1997). We also show a model with no applied force (Fig. 7a) to isolate the effect of gravity during this process, followed by the application of forces corresponding to pressures of 1 MPa, 2 MPa, and 5 MPa (Fig. 7b–d).

Following pressurisation, strain localises around the pre-existing weakness of the rheological boundary. In all cases, small scale rockfalls occur on the flanks of the dome, caused by over-steepening giving a high slope angle. Strain accumulates much deeper in the dome in all cases, highlighting development of deep-seated listric shear failure surfaces. The models subjected to both no and low (1 MPa) pressurisation effects show strain accumulation primarily localised at the corners of the core-talus interface, and in isolated regions along the rheological boundary. Domes subjected to higher pressurisation effects (2 MPa, 5 MPa) have more focussed bands of high strain, but these remain located along the boundary.

3.4. Sensitivity of pressurisation models to conduit diameter

The dome emplaced with a 50 m conduit diameter is shown in Fig. 8, after application of an equivalent 5 MPa pressure. This shows the same scenario as Fig. 7d, and displays very similar strain accumulation to the model with a 20 m conduit. Although the explicit values of strain are lower in the larger dome (~50% of those in the smaller dome), we still see that strain accumulates along the core/talus boundary, and then within the core of the dome. In the larger dome model, there is strain accumulation oblique to the listric shear plane, which has been observed in previous DEM models of rock slope instability (Wang et al., 2003).

3.5. Switch in extrusion direction

A switch in extrusion direction, or a focussed extrusion direction, has been documented as a precursor to collapse (Ryan et al., 2010; Stinton et al., 2014; Wadge et al., 2014), particularly at SHV due to the high quality of observations. There is no consensus on a proposed mechanism however, and switching extrusion direction has not previously been incorporated into numerical or analogue models. A focussed extrusion direction was observed during growth of the 2004–2006 lava dome complex at Mount St. Helens (Vallance et al., 2008). Due to cooling of older 2004–2005 dome rock, later spines experienced “thrusting

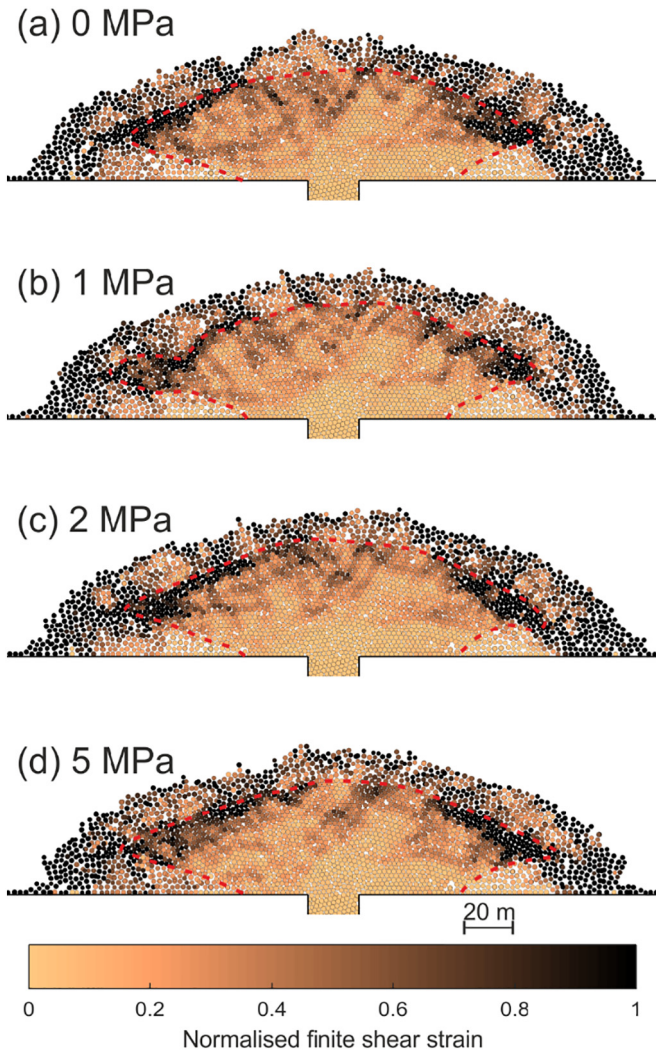


Fig. 7. PFC dome model following application of an upward force corresponding to pressures of (a) 0 MPa, (b) 1 MPa, (c) 2 MPa, (d) 5 MPa. Plotted using normalised finite shear strain, where the red dotted line represents the rheological interface between core and talus. Solidus pressure = 0.4 MPa.

growth” and were emplaced on top of earlier spines. The morphology of older spines and decoupling of later spines led to extrusion of younger spines oblique to horizontal, at angles up to 54°.

We implement a change in extrusion direction in the model by pausing active emplacement and freezing part of the dome. Displacements in the “frozen” part of the dome are set to zero to simulate material that has solidified. Once extrusion is resumed, the new material is forced

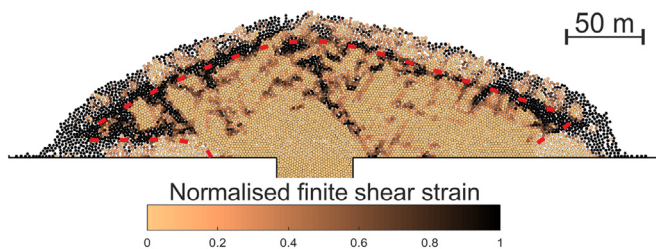


Fig. 8. PFC dome model with a 50 m conduit after application of force corresponding to 1 MPa pressure, plotted using normalised shear strain, where the red dotted line represents the rheological interface between core and talus. Solidus pressure = 0.4 MPa.

to extrude in a particular direction as it is prevented from spreading naturally by the frozen dome portion.

The results (Fig. 9) show firstly a large amount of shear strain localised above the conduit exit. Some of this strain accumulates due to fresh material moving alongside the frozen, older dome material. There is however significant strain accumulation in the form of shear bands on both sides of the conduit exit, a feature previously modelled by Hale and Wadge (2008). Strain is also localised along the lower rheological interface (Fig. 9c) between the core and talus on the non-frozen side of the dome. Strain accumulates towards the top of the dome sub-parallel to the rheological boundary (Fig. 9d), suggesting formation of a lava lobe that is being pushed out by incoming material; similar processes were observed in the DEM studies of Husain et al. (2018). This is significant in understanding future dome growth and morphology as we observe simulated cooling of one part of the dome to lead to lava lobe formation. The development of a deep, sub-horizontal shear band (Fig. 9d) is important for dome stability as it forms a potential failure surface (discussed further in Section 4.2). In terms of collapse style, rockfalls are seen to develop progressively throughout time following the focussed extrusion direction, occurring primarily on the over-steepened flanks of the dome.

3.6. Topographic effects

Topographic confinement of domes has been observed to control material detachment and pyroclastic flow generation (e.g. Voight et al., 2002). Previous dome growth models inadequately incorporate non-horizontal extrusion planes in controlling dome growth and talus generation, despite field observations of topography's influence (e.g. stiff crater walls buttressing dome emplacement (Hutchison et al., 2013)). Collapses occurring at Montserrat 1995–1997 were often due to dome material over-spilling the previous crater walls (Cole et al., 1998, 2002). We therefore create three end member topographies to test how dome morphology changes in each case. These are: magma extruding onto a slope (Fig. 10a); out of a conduit flanked by outward dipping slopes (Fig. 10b); and into a crater (Fig. 10c).

The dome extruded onto a slope shows strain accumulation on the downhill flank (Fig. 10a). Interestingly there is little strain accumulation on the uphill portion of the dome, despite the over-steepened flank, suggesting movement as a block and absence of rockfalls. Emplacing the dome at the apex of a flanked topography (Fig. 10b) and into a crater (Fig. 10c) both show rockfall activity on both slopes. For the crater case, most strain accumulation is seen in areas where the dome has overtopped the older crater rim (Fig. 10c), suggesting an abrupt change in slope leads to the highest strains. Additionally we see development of several subvertical fractures in the dome core (Fig. 10c). The development of these large scale features is not observed in the other modelled topographies but could have implications when considering overall material strength.

Due to randomness introduced by initial material packing, our modelled domes grow asymmetrically. This is shown particularly in the crater topography model where the rheological boundary location differs either side of the dome – core material is underlain by talus on one side, but is in contact with the crater on the other (Fig. 10c). The model presented in Fig. 10b also shows dome asymmetry, where the degree of over-steepening differs on each side.

4. Discussion

4.1. Shear band development

The development of shear bands in a material indicates a concentrated region of relatively high displacement. When analysing lava dome morphology, these regions aid identification of potential failure surfaces, where deformation accumulates to generate zones of weakness. In the model that simulates a focussed extrusion direction

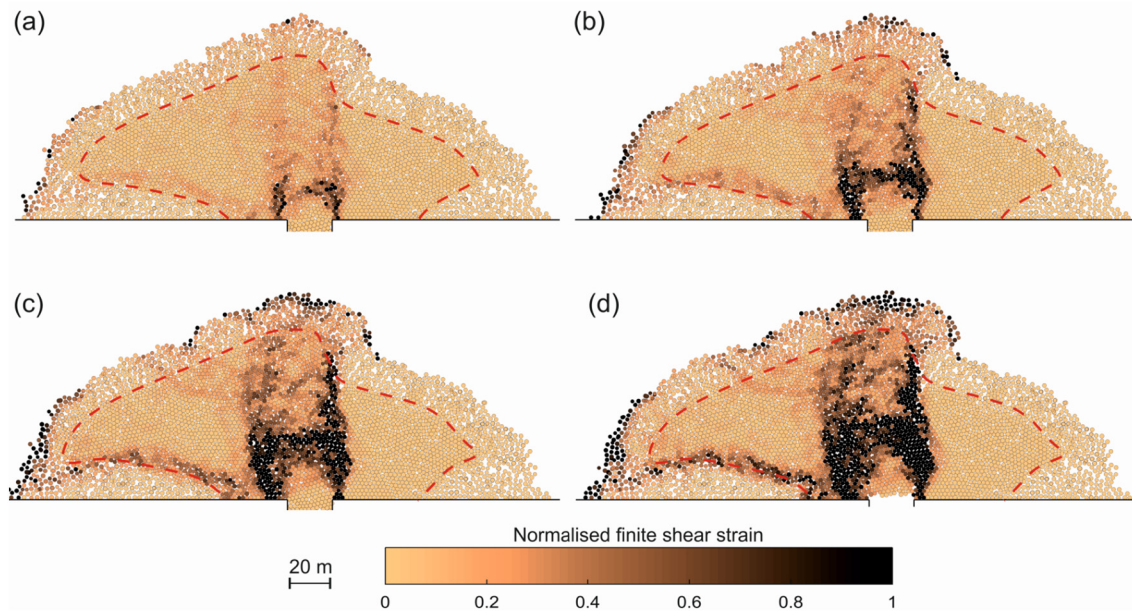


Fig. 9. PFC dome model, plotted using normalised finite shear strain, where the red dotted line represents the rheological interface between core and talus material. Insets (a) to (d) represent snapshots of increasing model run time. Solidus pressure = 0.4 MPa.

(Fig. 9), significant strain accumulation occurs around the conduit exit. In models from previous studies (e.g. Hale and Wadge, 2008), shear bands occur at the junction between the conduit and base of the dome, as they nucleate where new lava is emplaced adjacent to older lava. Shear band generation can be a precursor to a transition from exogenous to endogenous growth (i.e. magma forces its way to the surface to create lobes/spines rather than growth caused by magma intrusion and dome expansion (Calder et al., 2015; Fink et al., 1990)); this is implied further by propagation of shear bands towards the dome surface over time (Fig. 9d). Similar processes were seen by Buisson and Merle (2002), where analogue modelling of dome emplacement revealed that the zone of maximum strain, velocity, and displacement is observed directly above the conduit exit. Cordonnier et al. (2009) suggest shearing at the conduit exit can lead to spine formation. The development of shear bands in our PFC model is exaggerated due to the high extrusion rate; these results should therefore be seen as qualitative of process, rather than quantitative. Nevertheless we clearly see that a change in extrusion direction leads to strain accumulation in the centre of the dome that can be interpreted as carving out a pathway for lava to reach the surface and begin exogenous dome growth. This is not observed in the dome that is allowed to spread continuously.

In several models, deep accumulation of shear stress is clearly visible within the dome, whether this is purely along the core/talus boundary (Fig. 9) or intersecting the core (e.g. Fig. 7). In either case this shear accumulation marks localisation of displacement and development of a plane of weakness along which material can easily slide or be pushed out of the dome. These zones therefore demonstrate preferential dome cooling can cause lava lobe formation, often leading to over-steepened flow fronts which can collapse.

4.2. Developing pressurisation

Due to computational expense we model the pressurisation of the system separately from extrusion. The model with a purely gravitational response (i.e. no simulated pressurisation) shows that strain accumulates at the rheological boundary due to gravitational settling (Fig. 7a), but is intensified and focussed by addition of gas pressure (Fig. 7b–d). A natural next step would be to model gas pressure and extrusion as combined processes. We speculate that there would be more outwards

movement of talus slopes due to the combined effects of pressurisation and the lateral force of magma influx.

We demonstrate a simple way to add a pressure into a DEM model and complexities could be added to this in future model iterations. For example, the material in our model is allowed to deform, representing an open system that prohibits accumulation of gas pressure within the dome. An alternative scenario could be a dome with a “sealed cap” which cannot deform and allows a build-up of pressure. Equally it could be possible that a dome experiences reduction in pressure over time, for example due to evolution in the mechanical properties (e.g. permeability, fracturing) of the talus (Sparks, 1997). In the models presented here, the amount of shear strain accumulation shows significant material deformation and is therefore irreversible. Our models are acting beyond the elastic regime, and potential failure planes developed would continue to exist as weaknesses in the dome following reduction in pressure.

4.3. Model validation and similarity to conventional landslide studies

It is particularly challenging to validate our failure models, as dome collapse tends to culminate in explosive events. The only method to attempt to understand collapse process is examination of resultant deposits (normally block-and-ash flows). This means that despite hazards associated with lava dome collapse, we do not fully understand strain accumulation in the critical stages prior to collapse. Our models allow us to see a simplified cross-section through the dome interior and begin to reveal methods by which strain accumulates and alters the behaviour and stability state of a lava dome. We find that despite the complex conditions that exist during active lava dome growth (high temperatures, gas overpressure, seismicity), lava domes appear to behave in many ways similarly to traditional landslides – events that are commonly easier to observe than lava dome collapses. Particularly we see development of large scale listric shear planes, just as observed in rock or soil slope studies (e.g. Hungr et al., 2014; Petley et al., 2002). The actual slope failure process at a lava dome is difficult to discern due to the addition of gas resulting in turbulent pyroclastic density currents; it is therefore impossible to use the deposit to establish the way in which the slope failed (as in landslide studies) because the material completely disintegrates during the pyroclastic flow process. By

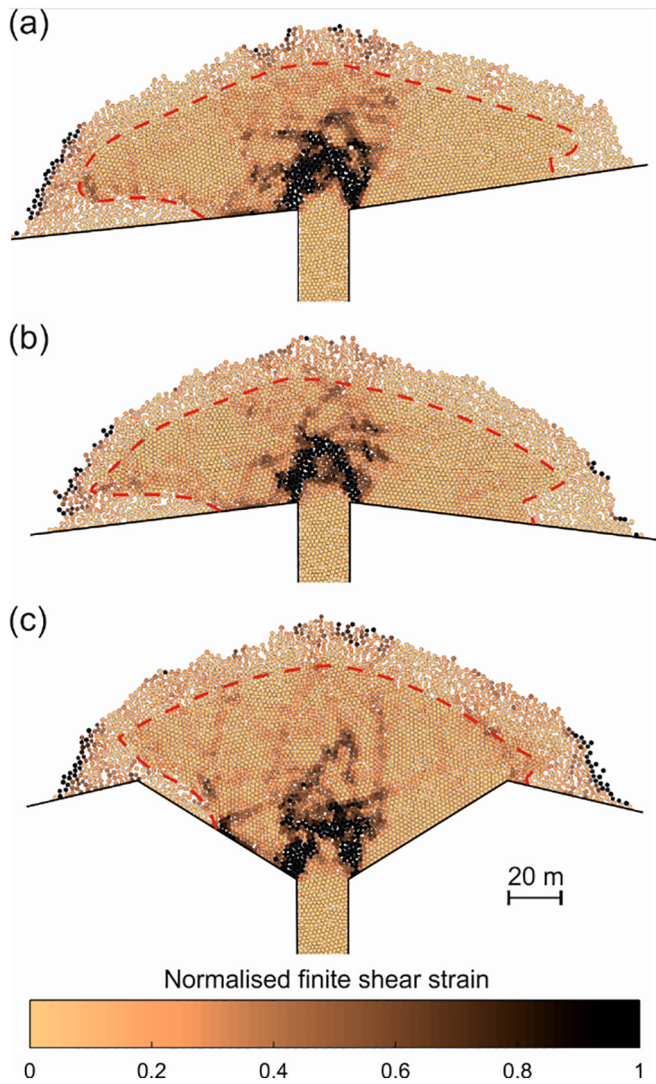


Fig. 10. PFC dome model extruded onto different surface topographies to represent (a) dome growth onto a slope; (b) growth out of a vent, onto sloped sides; (c) growth in a crater, where the dome eventually overtops crater walls. Rheological boundary between core and talus shown by red dotted line. Solidus pressure = 0.4 MPa.

using this modelling method to understand the generation of strain inside the lava dome, it reveals processes that cannot be otherwise discerned from observational studies.

4.4. Model development

We observe that failure plane development within pressurisation models (Fig. 7) is controlled primarily by the rheological boundary. We develop this hypothesis by pressurising domes emplaced with solidus pressures of 0.2 MPa and 0.8 MPa (Fig. 11). In the dome with a solidus pressure of 0.2 MPa (Fig. 11a), strain accumulates along the rheological boundary and we see a listric failure plane through the core of the right side of the dome. We suggest this is due to the low-angle dome morphology, preventing larger scale rockfalls in this area. In the dome with a solidus pressure of 0.8 MPa (Fig. 11b), strain accumulation reveals listric failure planes that also follow the rheological boundary, albeit deeper in the dome due to the larger talus volume. This sensitivity test shows the importance of solidus pressure in determining the volume of material involved in potential collapse, as it controls the depth at which the shear plane forms. We suggest therefore

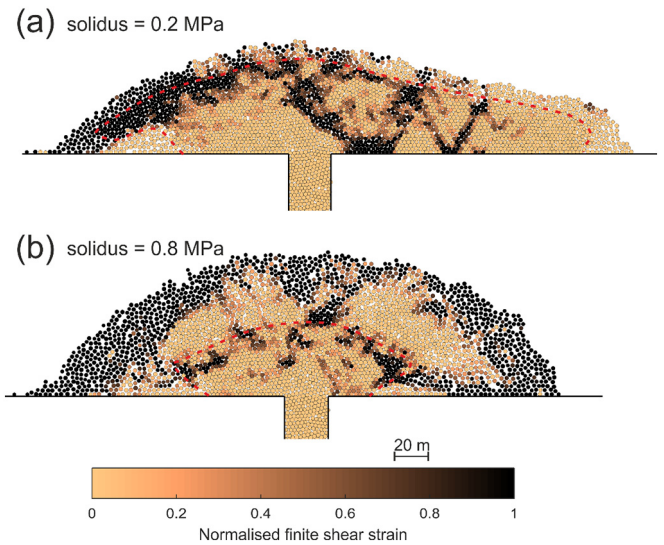


Fig. 11. PFC dome models, emplaced with solidus pressure of (a) 0.2 MPa and (b) 0.8 MPa. Both shown following the application of an upward force that corresponds to a pressure of 5 MPa, plotted using normalised shear strain, where the red dotted line represents the rheological interface between core and talus material.

that understanding the solidus pressure of a dome is key in assessing collapse hazard.

Following this, we propose that talus properties are crucial to the way in which shear accumulates around the rheological boundary. In all models presented here, we assume rock properties based on initial bond properties of the lava. Laboratory testing can determine mechanical properties of the talus material (e.g. Heap et al., 2014, 2016; Smith et al., 2011), however these sample-scale properties must be scaled before they can be applied to a volcano-scale model. Despite previous studies investigating this relationship at specific volcanic sites (Apuni et al., 2005; Okubo, 2004; Thomas et al., 2004; Watters et al., 2000), there is no general rule for taking intact laboratory strength and scaling it to rock mass strength in a volcanic environment. The same can be said for understanding elastic moduli at the scale of a volcanic edifice (Heap et al., 2018). A further degree of complexity is introduced in order to generate this calibrated, scaled material within PFC. Fully-scaled talus properties are therefore outside of the scope of this paper, but will be an important step in future model development.

5. Conclusions

We employed a discrete element method to develop lava dome models, and were able to simulate two distinct failure mechanisms: (1) shallow, superficial rockfalls and (2) deep-seated listric shear planes. The information that crater-confined domes lead primarily to superficial rockfalls has the potential to feed into hazard assessment, as models show these collapses to be shallow and relatively low in volume. We showed also that solidus pressure can control the volume of material involved in collapse. However it is important to recognise that trigger mechanisms can act simultaneously to destabilise a dome, a detail future models should consider. Deep-seated listric failure planes are observed following cessation of extrusion and subsequent generation of internal pressure. A collapse of this nature could lead to hot magma in the core being exposed to atmospheric pressure resulting in rapid decompression, explosions and pyroclastic flow generation. Deep shear planes also develop in models simulating switches in extrusion direction, although these are planar in nature and occur along the rheological boundary, showing lava lobe formation which can later lead to collapse.

Through knowledge of lava viscosity and extrusion conditions at a given lava dome, our method can be adapted in other locations to model dome morphology, and therefore propensity of the dome to collapse. Here we focus on pressurisation of the dome system, a non-horizontal underlying topography, or a change in extrusion direction, but many more scenarios could be analysed in this type of model. By visualising the strain within the dome and showing similar features to those observed in traditional landslide studies, we can begin to use knowledge of landslide processes to better understand the dome collapse process.

The models presented here use an innovative method to examine lava dome collapse, and provide a basic framework to understand the complex physics of a dynamically evolving system. Many additional factors can now be incorporated into future models to provide a more comprehensive understanding of factors likely to influence the stability of a growing lava dome. These include, for example, talus properties calibrated to real dome rock, a fracture network, successive extrusion events, and spatial/temporal variation in mechanical properties. We demonstrated that using discrete element method modelling is a promising approach for visualising strain generation within a lava dome, and interrogating the relationship between a growing dome and mechanisms that trigger instability.

Supplementary data to this article can be found online at <https://doi.org/10.1016/j.jvolgeores.2018.06.017>.

Acknowledgements

This work was supported by the Leeds York Spheres Doctoral Training Partnership (grant number NE/L002574/1). CEH also acknowledges the value of a place on the Itasca Educational Partnership, and therefore access to the PFC5.0 license. The authors would like to thank Martin Schöpfer and Dan Woodell for contribution of and assistance implementing the strain calculation code. The authors thank Mike Heap and an anonymous reviewer for helpful comments towards this manuscript, as well as Kelly Russell for editorial handling.

References

- Apuani, T., Corazzato, C., Cancelli, A., Tibaldi, A., 2005. Physical and mechanical properties of rock masses at Stromboli: a dataset for volcano instability evaluation. *Bull. Eng. Geol. Environ.* 64:419–431. <https://doi.org/10.1007/s10064-005-0007-0>.
- Ball, J.L., Stauffer, P.H., Calder, E.S., Valentine, G.A., 2015. The hydrothermal alteration of cooling lava domes. *Bull. Volcanol.* 77:102. <https://doi.org/10.1007/s00445-015-0986-z>.
- Blake, S., 1990. Viscoplastic models of lava domes. In: Fink, J.H. (Ed.), *Lava Flows and Domes: Emplacement Mechanisms and Hazard Implications*. Springer, Berlin Heidelberg, Berlin, Heidelberg, pp. 88–126. https://doi.org/10.1007/978-3-642-74379-5_5.
- Bourgouin, L., Hale, A.J., Arsac, A., 2007. Studying the Influence of a Solid Shell on Lava Dome Growth and Evolution Using the Level Set Method. pp. 1431–1438. <https://doi.org/10.1111/j.1365-246X.2007.03471.x>.
- Buisson, C., Merle, O., 2002. Experiments on internal strain in lava dome cross sections. *Bull. Volcanol.* 64:363–371. <https://doi.org/10.1007/s00445-002-0213-6>.
- Calder, E.S., Luckett, R., Sparks, R.S.J., Voight, B., 2002. Mechanisms of lava dome instability and generation of rockfalls and pyroclastic flows at Soufriere Hills Volcano, Montserrat. *Geol. Soc. Lond. Mem.* 21:173–190. <https://doi.org/10.1144/GSL.MEM.2002.021.01.08>.
- Calder, E.S., Lavallée, Y., Kendrick, J.E., Bernstein, M., 2015. Lava dome eruptions. The Encyclopedia of Volcanoes. Academic Press: pp. 343–362. <https://doi.org/10.1016/B978-0-12-385938-9.00018-3> (Chapter 18).
- Cardozo, N., Allmendinger, R.W., 2009. SSPX: a program to compute strain from displacement/velocity data. *Comput. Geosci.* 35:1343–1357. <https://doi.org/10.1016/j.cageo.2008.05.008>.
- Carn, S.A., Watts, R.B., Thompson, G., Norton, G.E., 2004. Anatomy of a lava dome collapse: the 20 March 2000 event at Soufriere Hills Volcano, Montserrat. *J. Volcanol. Geotherm. Res.* 100:241–264. [https://doi.org/10.1016/S0377-0273\(03\)00364-0](https://doi.org/10.1016/S0377-0273(03)00364-0).
- Cho, N., Martin, C.D., Segó, D.C., 2007. A clumped particle model for rock. *Int. J. Rock Mech. Min. Sci.* 44:997–1010. <https://doi.org/10.1016/j.ijrmms.2007.02.002>.
- Cole, P.D., Calder, E.S., Druitt, T.H., Hoblitt, R., Robertson, R., Sparks, R.S.J., Young, S.R., 1998. Pyroclastic flows generated by gravitational instability of the 1996–97 lava dome of Soufriere Hills Volcano, Montserrat. *Geophys. Res. Lett.* <https://doi.org/10.1029/98GL01510>.
- Cole, P.D., Calder, E.S., Sparks, R.S.J., Clarke, A., Druitt, T.H., Young, S.R., Herd, R.A., Harford, C.L., Norton, G.E., 2002. Deposits from dome-collapse and fountain-collapse pyroclastic flows at Soufriere Hills Volcano, Montserrat. *Geol. Soc. Lond. Mem.* 21, 231–262.
- Cordonnier, B., Hess, K.U., Lavallée, Y., Dingwell, D.B., 2009. Rheological properties of dome lavas: case study of Unzen volcano. *Earth Planet. Sci. Lett.* 279:263–272. <https://doi.org/10.1016/j.epsl.2009.01.014>.
- Cordonnier, B., Caricchi, L., Pistone, M., Castro, J., Hess, K., Gottschaller, S., Manga, M., Dingwell, D.B., 2012. The viscous-brittle transition of crystal-bearing silicic melt: direct observation of magma rupture and healing. *Geology* 40:611–614. <https://doi.org/10.1130/G3914.1>.
- Couch, S., Harford, C.L., Sparks, R.S.J., Carroll, M.R., 2003. *Experimental Constraints on the Conditions of Formation of Highly Calcic Plagioclase Microlites at the Soufriere Hills Volcano, Montserrat*. 44 pp. 1455–1475.
- Cundall, P.A., Strack, O.D.L., 1979. A discrete numerical model for granular assemblies. *Geotechnique* 29, 47–65.
- Darmawan, H., Walter, T.R., Sri, K., Made, I.G., Nandaka, A., 2018. Morphological and structural changes at the Merapi lava dome monitored in 2012–15 using unmanned aerial vehicles (UAVs). *J. Volcanol. Geotherm. Res.* 349:256–267. <https://doi.org/10.1016/j.jvolgeores.2017.11.006>.
- Dzurisin, D., Denlinger, R.P., Rosenbaum, J.G., 1990. Cooling rate and thermal structure determined from progressive magnetization of the Dacite Dome at Mount St. Helens, Washington. *J. Geophys. Res.* 95:2763. <https://doi.org/10.1029/JB095iB03p02763>.
- Elsworth, D., Voight, B., 2001. The mechanics of harmonic gas pressurization and failure of lava domes. *Geophys. J. Int.* 145:187–198. <https://doi.org/10.1046/j.1365-246x.2001.00370.x>.
- Elsworth, D., Voight, B., Thompson, G., Young, S.R., 2004. Thermal-hydrologic mechanism for rainfall-triggered collapse of lava domes. *Geology* 32:969–972. <https://doi.org/10.1130/G20730.1>.
- Fink, J.H., Malin, M.C., Anderson, S.W., 1990. Intrusive and extrusive growth of the Mount St Helens lava dome. *Nature* 348:435–437. <https://doi.org/10.1038/348435a0>.
- Gudmundsson, M.T., Jónsdóttir, K., Hooper, A., Holohan, E.P., Halldórsson, S.A., Ófeiggsson, B.G., Cesca, S., Vogfjörð, K.S., Sigmundsson, F., Högnadóttir, T., Einarsson, P., Sigmarrson, O., Jarosch, A.H., Jónasson, K., Magnússon, E., Hreinsdóttir, S., Bagnardi, M., Parks, M.M., Hjörleifsdóttir, V., Pálsson, F., Walter, T.R., Schöpfer, M.P.J., Heimann, S., Reynolds, H.I., Dumont, S., Bali, E., Gudfinnsson, G.H., Dahm, T., Roberts, M.J., Hensch, M., Belart, J.M.C., Spaans, K., Jakobsson, S., Gudmundsson, G. B., Fridriksdóttir, H.M., Drouin, V., Dürig, T., Aðalgeirsdóttir, G., Riishuus, M.S., Pedersen, G.B.M., van Boeckel, T., Oddsson, B., Pfeffer, M.A., Barsotti, S., Bergsson, B., Donovan, A., Burton, M.R., Aiuppa, A., 2016. Gradual caldera collapse at Bárðarbunga volcano, Iceland, regulated by lateral magma outflow. *Science* 353:aaf8988. <https://doi.org/10.1126/science.aaf8988> (80–).
- Hale, A.J., 2008. Lava dome growth and evolution with an independently deformable talus. *Geophys. J. Int.* 174:391–417. <https://doi.org/10.1111/j.1365-246X.2008.03806.x>.
- Hale, A.J., Wadge, G., 2005. *Computationally Modelling the Lava Dome at Soufriere Hills Volcano*. The University of Reading.
- Hale, A.J., Wadge, G., 2008. The transition from endogenous to exogenous growth of lava domes with the development of shear bands. *J. Volcanol. Geotherm. Res.* 171: 237–257. <https://doi.org/10.1016/j.jvolgeores.2007.12.016>.
- Hale, A.J., Bourgouin, L., Mühlhaus, H.B., 2007. Using the level set method to model endogenous lava dome growth. *J. Geophys. Res.* 112, B03213. <https://doi.org/10.1029/2006JB004445>.
- Hale, A.J., Calder, E.S., Loughlin, S.C., Wadge, G., Ryan, G.A., 2009a. Modelling the lava dome extruded at Soufriere Hills Volcano, Montserrat, August 2005–May 2006. Part I: dome shape and internal structure. *J. Volcanol. Geotherm. Res.* 187:69–84. <https://doi.org/10.1016/j.jvolgeores.2009.08.014>.
- Hale, A.J., Calder, E.S., Loughlin, S.C., Wadge, G., Ryan, G.A., 2009b. Modelling the lava dome extruded at Soufriere Hills Volcano, Montserrat, August 2005–May 2006. Part II: rockfall activity and talus deformation. *J. Volcanol. Geotherm. Res.* 187:69–84. <https://doi.org/10.1016/j.jvolgeores.2009.08.014>.
- Heap, M.J., Lavallée, Y., Petrakova, L., Baud, P., Reuschlé, T., Varley, N.R., Dingwell, D.B., 2014. Microstructural controls on the physical and mechanical properties of edifice-forming andesites at Volcán de Colima, Mexico. *J. Geophys. Res. Solid Earth* 119:2925–2963. <https://doi.org/10.1002/2013JB010521>.
- Heap, M.J., Russell, J.K., Kennedy, L.A., 2016. Mechanical behaviour of dacite from Mount St. Helens (USA): a link between porosity and lava dome extrusion mechanism (dome or spine)? *J. Volcanol. Geotherm. Res.* 328, 159–177.
- Heap, M., Villeneuve, M., Farquharson, J., Albino, F., Brothelande, E., Got, J.-L., 2018. Towards more realistic values of elastic moduli for volcano modelling. *Geophysical Research Abstracts*. EGU General Assembly Vienna 2018.
- Herd, R.A., Edmonds, M., Bass, V., 2005. Catastrophic lava dome failure at Soufriere Hills Volcano, Montserrat, 12–13 July 2003. *J. Volcanol. Geotherm. Res.* 148:234–252. <https://doi.org/10.1016/j.jvolgeores.2005.05.003>.
- Holohan, E.P., Schöpfer, M.P.J., Walsh, J.J., 2011. Mechanical and geometric controls on the structural evolution of pit crater and caldera subsidence. *J. Geophys. Res. Solid Earth* 116:1–23. <https://doi.org/10.1029/2010JB008032>.
- Holohan, E.P., Schöpfer, M.P.J., Walsh, J.J., 2015. Stress evolution during caldera collapse. *Earth Planet. Sci. Lett.* 421:139–151. <https://doi.org/10.1016/j.epsl.2015.03.003>.
- Hungr, O., Leroueil, S., Picarelli, L., 2014. The Varnes classification of landslide types, an update. *Landslides* 11:167–194. <https://doi.org/10.1007/s10346-013-0436-y>.
- Husain, T., Elsworth, D., Voight, B., Mattioli, G.S., Jansma, P., 2014. Influence of extrusion rate and magma rheology on the growth of lava domes: insights from particle-dynamics modeling. *J. Volcanol. Geotherm. Res.* 285:110–117. <https://doi.org/10.1016/j.jvolgeores.2014.08.013>.
- Husain, T., Elsworth, D., Voight, B., Mattioli, G., Jansma, P., 2018. Influence of conduit flow mechanics on magma rheology and the growth style of lava domes. *Geophys. J. Int.* 213:1768–1784. <https://doi.org/10.1093/gji/ggy073>.
- Hutchison, W., Varley, N., Pyle, D.M., Mather, T.A., Stevenson, J.A., 2013. Airborne thermal remote sensing of the Volcán de Colima (Mexico) lava dome from 2007 to 2010. *Geol. Soc. Lond. Spec. Publ.* 380:203–228. <https://doi.org/10.1144/SP380.8>.

- Itasca Consulting Group, I, 2017. PFC2D (Particle Flow Code in Two Dimensions).
- Jaeger, J., Cook, N., Zimmerman, R., 2009. *Fundamentals of Rock Mechanics*. John Wiley & Sons.
- Jenck, O., Dias, D., Kastner, R., 2009. Discrete element modelling of a granular platform supported by piles in soft soil - validation on a small scale model test and comparison to a numerical analysis in a continuum. *Comput. Geotech.* 36:917–927. <https://doi.org/10.1016/j.compgeo.2009.02.001>.
- Loughlin, S.C., Luckett, R., Ryan, G., Christopher, T., Hards, V., De Angelis, S., Jones, L., Strutt, M., 2010. An overview of lava dome evolution, dome collapse and cyclicity at Soufriere Hills Volcano, Montserrat, 2005–2007. *Geophys. Res. Lett.* 37. <https://doi.org/10.1029/2010GL042547>.
- Matthews, A.J., Barclay, J., 2004. A thermodynamical model for rainfall-triggered volcanic dome collapse. *Geophys. Res. Lett.* 31. <https://doi.org/10.1029/2003GL019310>.
- Matthews, A.J., Barclay, J., Carn, S.A., Thompson, G., Alexander, J., Herd, R.A., Williams, C., 2002. Rainfall-induced volcanic activity on Montserrat. *Geophys. Res. Lett.* 29. <https://doi.org/10.1029/2002GL014863>.
- Melnik, O., Sparks, R.S.J., 2002. Dynamics of magma ascent and lava extrusion at Soufrière Hills Volcano, Montserrat. *Geol. Soc. Lond. Mem.* 21:153–171. <https://doi.org/10.1144/GSL.MEM.2002.021.01.07>.
- Melnik, O., Sparks, R.S.J., 2005. Controls on conduit magma flow dynamics during lava dome building eruptions. *J. Geophys. Res. B Solid Earth* 110:1–21. <https://doi.org/10.1029/2004JB003183>.
- Moore, G., Vennemann, T., Carmichael, I.S.E., 1998. An empirical model for the solubility of H₂O in magmas to 3 kilobars. *Am. Mineral.* 83:36–42. <https://doi.org/10.1016/j.jvolgeores.2004.09.019>.
- Morgan, J.K., McGovern, P.J., 2005a. Discrete element simulations of gravitational volcanic deformation: 1. Deformation structures and geometries. *J. Geophys. Res. B Solid Earth* 110:1–22. <https://doi.org/10.1029/2004JB003252>.
- Morgan, J.K., McGovern, P.J., 2005b. Discrete element simulations of gravitational volcanic deformation: 2. mechanical analysis. *J. Geophys. Res. B Solid Earth* 110:1–13. <https://doi.org/10.1029/2004JB003253>.
- Ogburn, S.E., Loughlin, S.C., Calder, E.S., 2015. The association of lava dome growth with major explosive activity (VEI≥4): DomeHaz, a global dataset. *Bull. Volcanol.* 77. <https://doi.org/10.1007/s00445-015-0919-x>.
- Okubo, C.H., 2004. Rock mass strength and slope stability of the Hilina slump, Kilauea volcano, Hawai'i. *J. Volcanol. Geotherm. Res.* 138:43–76. <https://doi.org/10.1016/j.jvolgeores.2004.06.006>.
- Osher, S., Sethian, J.A., 1988. Fronts propagating with curvature-dependent speed: algorithms based on Hamilton-Jacobi formulations. *J. Comput. Phys.* 79:12–49. [https://doi.org/10.1016/0021-9991\(88\)90002-2](https://doi.org/10.1016/0021-9991(88)90002-2).
- Petley, D.N., Bulmer, M.H., Murphy, W., 2002. Patterns of movement in rotational and translational landslides. *Geology* 30:719–722. [https://doi.org/10.1130/0091-7613\(2002\)030<0719:POMIRA>2.0.CO;2](https://doi.org/10.1130/0091-7613(2002)030<0719:POMIRA>2.0.CO;2).
- Potyondy, D.O., 2012. A Flat-jointed Bonded-particle Material for Hard Rock. 46th US Rock Mech. Symp. 10.
- Potyondy, D., 2016. Material-Modeling Support in PFC [via fistPkg20].
- Robertson, R., Cole, P.D., Sparks, R.S.J., Harford, C., Lejeune, A.M., Miller, A.D., Murphy, M. D., Norton, G., Stevens, N.F., 1998. The explosive eruption of Soufriere Hills Volcano, Montserrat, West Indies, 17 September, 1996. *Geophys. Res. Lett.* 25, 3429–3432.
- Ryan, G.A., Loughlin, S.C., James, M.R., Jones, L., Calder, E.S., Christopher, T., Strutt, M., Wadge, G., 2010. Growth of the lava dome and extrusion rates at Soufriere Hills Volcano, Montserrat, West Indies: 2005–2008. *Geophys. Res. Lett.* 37. <https://doi.org/10.1029/>
- Sato, H., Fujii, T., Nakada, S., 1992. Crumbling of dacite dome lava and generation of pyroclastic flows at Unzen volcano. *Lett. Nat.* 360, 664–666.
- Schöpfer, M.P.J., Childs, C., Walsh, J.J., 2006. Localisation of normal faults in multilayer sequences. *J. Struct. Geol.* 28:816–833. <https://doi.org/10.1016/j.jsg.2006.02.003>.
- Simmons, J., Elsworth, D., Voight, B., 2005. Classification and idealized limit-equilibrium analyses of dome collapses at Soufrière Hills volcano, Montserrat, during growth of the first lava dome: November 1995–March 1998. *J. Volcanol. Geotherm. Res.* 139: 241–258. <https://doi.org/10.1016/j.jvolgeores.2004.08.009>.
- Smith, R., Sammonds, P.R., Tuffen, H., Meredith, P.G., 2011. Evolution of the mechanics of the 2004–2008 Mt. St. Helens lava dome with time and temperature. *Earth Planet. Sci. Lett.* 307:191–200. <https://doi.org/10.1016/j.epsl.2011.04.044>.
- Sparks, R.S.J., 1997. Causes and consequences of pressurisation in lava dome eruptions. *Earth Planet. Sci. Lett.* 150, 177–189.
- Sparks, R.S.J., Murphy, M.D., Lejeune, A.M., Watts, R.B., Barclay, J., Young, S.R., 2000. Control on the emplacement of the andesitic lava dome of the Soufriere Hills Volcano, Montserrat by degassing-induced crystallization. *Terra Nova* 12, 14–20.
- Stinton, A.J., Cole, P.D., Stewart, R.C., Odbert, H.M., Smith, P., 2014. The 11 February 2010 partial dome collapse at Soufriere Hills Volcano, Montserrat. *Geol. Soc. Lond. Mem.* 39:133–152. <https://doi.org/10.1144/M39.7>.
- Swanson, D.A., Dzurisin, D., Holcomb, R.T., Iwatsubo, E.Y., Chadwick, W.W., Casadevall, T.J., Ewert, J.W., Heliker, C.C., 1987. Growth of the lava dome at Mount St. Helens, Washington, (USA), 1981–1983. *Geol. Soc. Am. Spec. Pap.* 212, 1–16.
- Taron, J., Elsworth, D., Thompson, G., Voight, B., 2007. Mechanisms for rainfall-concurrent lava dome collapses at Soufrière Hills Volcano, 2000–2002. *J. Volcanol. Geotherm. Res.* 160:195–209. <https://doi.org/10.1016/j.jvolgeores.2006.10.003>.
- Thomas, M.E., Petford, N., Bromhead, E.N., 2004. Volcanic rock-mass properties from Snowdonia and Tenerife: implications for volcano edifice strength. *J. Geol. Soc. Lond.* 161:939–946. <https://doi.org/10.1144/0016-764903-166>.
- Vallance, J.W., Schneider, D.J., Schilling, S.P., 2008. Growth of the 2004–2006 Lava-Dome Complex at Mount St. Helens, Washington. A volcano rekindled renewed erupt. *Mt. St. Helens 2004–2006*, U.S. Geol. Surv. Prof. Pap. 1750, 169–208.
- Villemant, B., Mouatt, J., Michel, A., 2008. Andesitic magma degassing investigated through H₂O vapour-melt partitioning of halogens at Soufrière Hills Volcano, Montserrat (Lesser Antilles). *Earth Planet. Sci. Lett.* 269:212–229. <https://doi.org/10.1016/j.epsl.2008.02.014>.
- Voight, B., 2000. Structural stability of andesite volcanoes and lava domes. *Philos. Trans. R. Soc. Lond.* 358, 1663–1703.
- Voight, B., Elsworth, D., 2000. Instability and collapse of hazardous gas-pressurized lava domes. *Geophys. Res. Lett.* 27:1–4. <https://doi.org/10.1029/1999GL008389>.
- Voight, B., Hoblitt, R.P., Clarke, A.B., Lockhart, A.B., Miller, A.D., Lynch, L., McMahon, J., 1998. Remarkable cyclic ground deformation monitored in real-time on Montserrat, and its use in eruption forecastin. *Geophys. Res. Lett.* 25, 3405–3408.
- Voight, B., Sparks, R.S.J., Miller, A.D., Stewart, R.C., Hoblitt, R.P., Clarke, A., Ewart, J., Aspinall, W.P., Bapchie, B., Calder, E.S., Cole, P.D., Druitt, T.H., Hartford, C., Herd, R.A., Jackson, P., Lejeune, A.M., Lockhart, A.B., Loughlin, S.C., Luckett, R., Lynch, L., Norton, G.E., Robertson, R., Watson, I.M., Watts, R., Young, S.R., 1999. Magma flow instability and cyclic activity at Soufriere Hills volcano, Montserrat, British West Indies. *Science* (80-) 283, 1138–1142.
- Voight, B., Komorowski, J.-C., Norton, G.E., Belousov, A.B., Belousova, M., Boudon, G., Francis, P.W., Franz, W., Heinrich, P., Sparks, R.S.J., Young, S.R., 2002. The 26 December (Boxing Day) 1997 sector collapse and debris avalanche at Soufrière Hills Volcano, Montserrat. *Geol. Soc. Lond. Mem.* 21:363–407. <https://doi.org/10.1144/GSL.MEM.2002.021.01.17>.
- Voight, B., Linde, A.T., Sacks, I.S., Mattioli, G.S., Sparks, R.S.J., Elsworth, D., Hidayat, D., Malin, P.E., Shalev, E., Widiwijayanti, C., Young, S.R., Bass, V., Clarke, A., Dunkley, P., Johnston, W., McWhorter, N., Neuberger, J., Williams, P., 2006. Unprecedented pressure increase in deep magma reservoir triggered by lava-dome collapse. *Geophys. Res. Lett.* <https://doi.org/10.1029/2005GL024870>.
- Wadge, G., Macfarlane, D.G., Odbert, H.M., James, M.R., Hole, J.K., Ryan, G., Bass, V., De Angelis, S., Pinkerton, H., Robertson, D.A., Loughlin, S.C., 2008. Lava dome growth and mass wasting measured by a time series of ground-based radar and seismicity observations. *J. Geophys. Res. Solid Earth* 113:1–15. <https://doi.org/10.1029/2007JB005466>.
- Wadge, G., Ryan, G., Calder, E.S., 2009. Clastic and core lava components of a silicic lava dome. *Geology* 37:551–554. <https://doi.org/10.1130/G25747A.1>.
- Wadge, G., Herd, R.A., Ryan, G.A., Calder, E.S., Komorowski, J.C., 2010. Lava production at Soufriere Hills Volcano, Montserrat: 1995–2009. *Geophys. Res. Lett.* 37. <https://doi.org/10.1029/2009GL041466>.
- Wadge, G., Voight, B., Sparks, R.S.J., Cole, P.D., Loughlin, S.C., Robertson, R.E., 2014. An overview of the eruption of Soufriere Hills volcano, Montserrat from 2000 to 2010. *Geol. Soc. Lond. Mem.* 39:1–40. <https://doi.org/10.1144/M39.1>.
- Walter, T.R., Legrand, D., Granados, H.D., Reyes, G., Arámula, R., 2013. Volcanic eruption monitoring by thermal image correlation: pixel offsets show episodic dome growth of the Colima volcano. *J. Geophys. Res. Solid Earth* 118:1408–1419. <https://doi.org/10.1002/jgrb.50066>.
- Walter, T.R., Subandriyo, J., Kirbani, S., Bathke, H., Suryanto, W., Aisyah, N., Darmawan, H., Jousset, P., 2015. Tectonophysics volcano-tectonic control of Merapi ⁶⁶™ lava dome splitting : the November 2013 fracture observed from high resolution TerraSAR-X data. *Tectonophysics* 639:23–33. <https://doi.org/10.1016/j.tecto.2014.11.007>.
- Wang, Y., Tonn, F., 2009. Modeling Lac du Bonnet granite using a discrete element model. *Int. J. Rock Mech. Min. Sci.* 46:1124–1135. <https://doi.org/10.1016/j.ijrmm.2009.05.008>.
- Wang, C., Tannatt, D.D., Lilly, P.A., 2003. Numerical analysis of the stability of heavily jointed rock slopes using PFC2D. *Int. J. Rock Mech. Min. Sci.* 40:415–424. [https://doi.org/10.1016/S1365-1609\(03\)00004-2](https://doi.org/10.1016/S1365-1609(03)00004-2).
- Watters, R.J., Zimbelman, D.R., Bowman, S.D., Crowley, J.K., 2000. Rock mass strength assessment and significance to edifice stability, Mount Rainier and Mount Hood, Cascade range volcanoes. *Pure Appl. Geophys.* 157:957–976. <https://doi.org/10.1007/s000240050012>.
- Watts, R.B., Herd, R.A., Sparks, R.S.J., Young, S.R., 2002. Growth patterns and emplacement of the andesitic lava dome at Soufriere Hills Volcano, Montserrat. *Geol. Soc. Lond. Mem.* 21:115–152. <https://doi.org/10.1144/GSL.MEM.2002.021.01.06>.
- Wu, S., Xu, X., 2016. A study of three intrinsic problems of the classic discrete element method using flat-joint model. *Rock Mech. Rock Eng.* 49:1813–1830. <https://doi.org/10.1007/s00603-015-0890-z>.
- Zhang, Q., Zhu, H., Zhang, L., Ding, X., 2011. Study of scale effect on intact rock strength using particle flow modeling. *Int. J. Rock Mech. Min. Sci.* 48:1320–1328. <https://doi.org/10.1016/j.ijrmm.2011.09.016>.